Article

Molecular dynamics study on growth of carbon dioxide and methane hydrate from a seed crystal

Prajakta Nakate [1], Bappa Ghosh [2], Subhadip Das [3,*], Sudip Roy [2,*], Rajnish Kumar [4,*]

[1] Chemical Engineering and Process Development, National Chemical Laboratory, Pune 411008, India
[2] Physical and Materials Chemistry Division, National Chemical Laboratory, Pune 411008, India
[3] Department of Chemistry, Chaudhary Ranbir Singh University, Jind, Haryana-126102
[4] Department of Chemical Engineering, Indian Institute of Technology, Madras, Chennai 600036, Tamil Nadu, India

ABSTRACT

In the current work, molecular dynamics simulation is employed to understand the intrinsic growth of carbon dioxide and methane hydrate starting from a seed crystal of methane and carbon dioxide respectively. This comparison was carried out because it has relevance to the recovery of methane gas from natural gas hydrate reservoirs by simultaneously sequestering a greenhouse gas like CO_2. The seed crystal of carbon dioxide and methane hydrate was allowed to grow from a super-saturated mixture of carbon dioxide or methane molecules in water respectively. Two different concentrations (1:6 and 1:8.5) of CO_2/CH_4 molecules per water molecule were chosen based on gas–water composition in hydrate phase. The molecular level growth as a function of time was investigated by all atomistic molecular dynamics simulation under suitable temperature and pressure range which was well above the hydrate stability zone to ensure significantly faster growth kinetics. The concentration of CO_2 molecules in water played a significant role in growth kinetics, and it was observed that maximizing the CO_2 concentration in the aqueous phase may not result in faster growth of CO_2 hydrate. On the contrary, methane hydrate growth was independent of methane molecule concentration in the aqueous phase. We have validated our results by performing experimental work on carbon dioxide hydrate where it was seen that under conditions appropriate for liquid CO_2, the growth for carbon dioxide hydrate was very slow in the beginning.

© 2019 The Chemical Industry and Engineering Society of China, and Chemical Industry Press Co., Ltd.
All rights reserved.

1. Introduction

Gas hydrates are ice-like crystalline, non-stoichiometric inclusion compounds composed of organic/inorganic moieties which are trapped within the cages formed by a network of hydrogen-bonded water molecules. These water cages are formed by four, five and six membered hydrogen bonded rings which are interconnected *via* each other to form various types of crystalline structure [1,2]. There are three naturally abundant crystalline forms of gas hydrates namely structure I (sI, cubic type), structure II (sII, body-centered cubic type) and hexagonal structure (sH, face-centered cubic type). The sI unit cell has two 5^{12} and six $5^{12}6^2$ cages. Similarly, the sII unit cell has sixteen 5^{12} and eight $5^{12}6^4$ cages, and sH has three 5^{12}, two $4^35^6$$6^3$, and one $5^{12}6^8$ cages [3–6]. In the present work, we have dealt with structure I hydrates formed by carbon dioxide and methane independently.

Methane recovery from natural gas hydrate reserves by the injection of industrially emitted carbon dioxide is considered to be a promising approach as it provides the added impetus of simultaneously sequestering

extraneous CO_2. The method of recovering methane from natural gas hydrates by injection of carbon dioxide is a novel approach [7–10]. In 2011, a field trial done by Conoco Philips on Alaska North slope showed that through injection of carbon dioxide, it is possible to produce methane from natural gas hydrates and simultaneously sequester carbon dioxide. Several problems were observed from the field test such as difficulties related to injecting CO_2 into a less consolidated reservoir at low temperature and production of elevated levels of water and sand. Injection problem was later solved by adding a suitable concentration of N_2 since it reduced the density in the column [11]. However, one of the major concerns for the production of methane from natural gas hydrates by pumping carbon dioxide rich liquid phase was incomplete recovery of methane [12,13]. It is evident that optimum temperature and pressure condition necessary to maximize methane recovery is not available. However, for suggesting such thermodynamic conditions at macro scale one needs to understand the kinetics and mechanism of pure methane and pure carbon dioxide hydrate formation at a molecular level.

During hydrate formation, different phenomena *e.g.*, hydrate nucleation [14,15], cage dynamics in case of mixed hydrate [16], growth mechanism [17,18], kinetics of inhibition and promotion [19–21] occur at a shorter (atomistic scale) time and length scale.

* Corresponding authors.
  E-mail addresses: Subhadipdas@crsu.ac.in (S. Das), sroy@invictusoncology.com
(S. Roy), rajnish@iitm.ac.in (R. Kumar).

Molecular dynamics simulation has been extensively used to probe such events at that time scale and has proven to be an effective tool for detailed quantitative predictions of mechanisms. Walsh *et al.* [22] has investigated the methane hydrate nucleation and growth by molecular dynamics at suitable thermodynamic conditions of 250 K and 50 MPa. They found the coexistence of sI and sII structures despite there being a thermodynamic preference for sI. This was attributed to the kinetics of formation which governed the nucleation of hydrates involving methane and water. Sarupria and Debenedetti [23] illustrated the homogeneous nucleation of methane hydrate from bulk methane–water in the absence of interfaces. Hydrate like clusters were formed which did not possess the long range order as in methane hydrate. Apart from that, the ratio of the cages in clusters was less than that present in classic hydrate structures. Nada [24] simulated a three phase system of a gas, clathrate, and liquid water in order to investigate the growth mechanism of the clathrate. They reported that growth from the concentrated solution contained some empty cages while no such empty cages were seen in the case of growth from dilute solution. Tung *et al.* [25] studied the effect of pressure on the growth rate of methane hydrate. They reported that the growth rate depends on methane solubility in the water phase, diffusion of methane by mass transport and the affinity of methane to incomplete water cages at the interface. A significant amount of work has been done on the growth of methane hydrates while the formation and growth study for carbon dioxide hydrates are comparatively rare. Granasy *et al.* [26] studied nucleation and growth of carbon dioxide hydrates using phase field theory. Tung *et al.* [27] investigated growth of carbon dioxide hydrates over a wide range of pressures. They reported a new meta-stable medium sized $4^{1}5^{10}6^{2}$ cage at the hydrate growing interface and subsequent transformation of these cages into more stable sI hydrate. A significant work was done by Zhongjin *et al.* [28] where they performed microsecond molecular dynamics simulation to deal with carbon dioxide nucleation. They found out that the adsorption of CO_2 molecules around its own hydration shell is significant for stabilizing the hydrogen bond and hence in inducing the nucleation of CO_2 hydrate. Sarupria and Debenedetti [29] did another study where they investigated the effects of cage occupancy on the decomposition of CO_2 hydrate in the presence of amorphous water. They showed that it is important to consider the aspect of relative occupancy in large and small cages rather than the overall hydrate occupancy for studying the effect on CO_2 hydrate dissociation.

Carbon dioxide can replace the methane from the solid hydrate phase as it is thermodynamically favorable to form CO_2 hydrate compared to methane hydrate in a subsea environment. However, kinetics of hydrate formation and effect of pressure and resulting liquefaction of CO_2 on hydrate formation kinetics are not well known. Therefore we believe that, it is important to separately understand the gas hydrate formation from pure methane and pure carbon dioxide respectively. Bulk techniques such as gas uptake measurements are typically used for determining the kinetics of hydrate formation [30]. Such measurements suggest a relatively homogeneous process of gradual water to hydrate conversion. However, micro-imaging measurements on hydrate formation of pure methane and carbon dioxide have conclusively shown that at molecular level, conversion of liquid water drops to hydrate is quite inhomogeneous; within a very small reactor, some drops converted to hydrate in few minutes while others required hours or days. Thus quantitative measurements of kinetic processes in sub-volumes of a larger sample suggest that the smaller the volume observed, the more inhomogeneous the process appears to be [31]. The intriguing question is how this process of liquid to solid conversion happens in the presence of gases which has very limited solubility in each other. Hydrate may nucleate at the gas–water interface, however, subsequent hydrate growth must involve transport of either water or gas at the interface and it may depend on multiple parameters including the difference in hydrophobicities and by extension, polarities of CO_2 and CH_4. Thus their solubility in water would be very different which

would result in different growth kinetics. The consequences of these differences in hydrophobicity and polarity of the guest molecules (CO_2 and CH_4) on hydrate formation kinetics have been addressed in the present work.

We study the growth kinetics of pure carbon dioxide hydrate, and pure methane hydrate starting from a seed crystal under similar thermodynamic conditions. We have maintained a constant temperature and pressure in our simulation box to study the intrinsic growth of hydrate formation. Two different concentrations representing a supersaturated solution of carbon dioxide and methane were studied at multiple temperature and pressure, which was above the three-phase boundary of hydrate formation for achieving sustained hydrate growth. The growth mechanisms of these hydrates were analyzed and growth rates at two different concentrations, temperatures, and pressures were compared. The growth of crystal was monitored using order parameter (discussed in the results section).

2. Simulation procedure

Fig. 1 represents a typical hydrate two-phase simulation box, having CO_2 and CH_4 seed crystal (solid phase) located approximately in the middle of the simulation cell and CO_2 or CH_4 water mixture (liquid phase) on both sides of the hydrate phase in the Z-direction. The hydrate phase used in the study consisted of $3 \times 3 \times 6$ unit cell of structure I hydrate with all its cages filled with CO_2 or CH_4 (432 guest molecules and 2484 water molecules). The crystal structure was then randomly solvated with CO_2 gas molecules (and CH_4 gas for CH_4 hydrate) and water on both the sides in the Z-direction to get the final simulation box as shown in ESI (Fig. S1).

MD simulations were carried out by changing the concentration of hydrate forming gas in the aqueous phase. Two different concentrations (1:6 and 1:8.5 mol ratio of CH_4/CO_2 water) used in this study represent a typical gas to water mole ratio for methane and carbon dioxide hydrate respectively. The ratio of 1:6 suggests 1 mole of hydrate forming gas for every 6 moles of water; this concentration is very close to the hydration number of structure I hydrate. Gas molecules were randomly placed in the aqueous phase and the system was equilibrated for a short time at hydrate forming thermodynamic condition (Table 1 for details). The temperature and pressure conditions chosen for this work were above the solid–liquid coexistence line in the three phase diagram of pure methane and CO_2 hydrate (see ESI fig. S2). After equilibration, it is noted that the simulation box appears quite different for both the systems (CH_4 and CO_2 system) in terms of distribution of gases in the aqueous phase, however, to compare the growth kinetics of pure CH_4 and pure CO_2 hydrate all the production runs were carried out under same concentration.

Production run simulations were performed using GROMACS 4.5.5 software package [32]. The TIP4P/ICE (for water) [33,34], EPM2 (for carbon dioxide) [35,36] and OPLS-UA (for methane) [37] force-field models were considered for all the simulations. The geometric combination rule was used to calculate LJ parameters between the atoms of carbon dioxide–water and methane–water. The detailed force field parameters are given in Table S2. The leapfrog algorithm was used to integrate the equations of motion with a time step of 1 fs for both NVT and NPT runs. The LINCS algorithm was used to constrain the bond length between the atoms in rigid molecules [38]. The cut-off distance of 1.2 nm was taken to calculate the short-range non-bonded interactions. Particle Mesh Ewald (PME) summations were used for calculating the coulombic long range interactions with a relative Ewald tolerance of 1×10^{-6} [39,40].

The simulation box with periodic boundary conditions was simulated following the procedure described below. Initially, a short equilibration run was carried out for 1 ns in NVT ensemble followed by 5 ns in NPT ensemble with the position restrained hydrate seed crystal to minimize the interfacial energy of solid–liquid boundary. The equilibrated structure was then subjected to the final production run in the
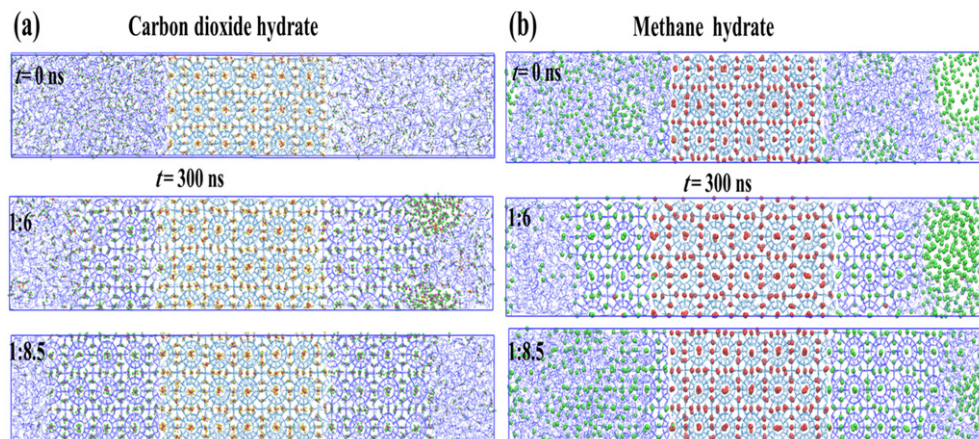
Fig. 1. (a) Snapshots of carbon dioxide–water system at the beginning ($t = 0$ ns) and at the end (300 ns) of NPT production run for 1:6 and 1:8.5 ratio of CO_2 and water. (Cyan — hydrate water, blue — amorphous water, red and yellow — carbon and oxygen of carbon dioxide in hydrate phase, purple and green — carbon and oxygen of carbon dioxide in amorphous phase.) (b) Snapshots of methane-water system at the beginning ($t = 0$ ns) and at the end (300 ns) of NPT production run for 1:6 and 1:8.5 ratio of CH_4 and water. It is noted that the pressure and temperature conditions were same in both the systems (50 MPa and 260 K). (Red — united atom methane in hydrate phase, green — united atom methane in amorphous phase, cyan — hydrate water, blue — amorphous water.)

NPT ensemble. The Nose–Hoover temperature thermostat [41,42] with a relaxation time of 0.5 ps and Parrinello–Rahman pressure barostat [43,44] with a relaxation time of 1 ps were used for each thermodynamic condition as given in Table 1. Semi-isotropic pressure coupling was used such that the box length scaled along the z-dimension (direction of crystal growth) independent of the x–y direction with a coupling time of 1.00 ps. All the simulations were repeated from scratch (*i.e.*, building the amorphous water–CO_2 and water–CH_4 phase) three times, and the average results were plotted for further analysis.
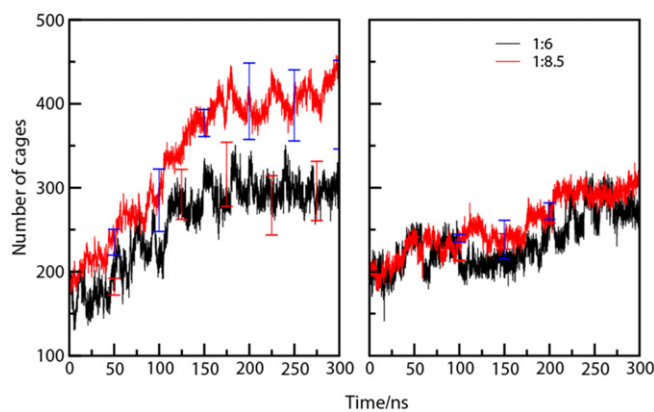
3. Algorithm for determination of cages

Number of cages during hydrate growth can be monitored through accounting the large and small cages by analyzing the trajectory as proposed by Jacobson *et al.* [45]. The algorithm first looks for all the oxygen atoms which are within 0.61 nm of a guest molecule *i.e.*, carbon dioxide or methane molecule. In the above criteria it is assumed that a guest molecule which is present anywhere in the cage (at the edge of the cage) will also get counted and be part of the system. With the information on the structure of the water molecules in hydrate form and the topology of the rings they form in structure I hydrate [46], a criterion is selected for the connectivity of oxygen atoms, which is 0.35 nm apart from each other. In the second stage of the algorithm, the search is initiated for possible pentagonal and hexagonal rings which are formed by connecting identified oxygen atoms. The given procedure is used to identify 5^{12} and $5^{12}6^2$ cages composed of 20 and 24 water molecules [47].

4. Results and Discussion

Table 1 summarizes the simulation conditions such as concentration, pressure and temperature used in this study. The pressure and

Table 1
Systems studied in this work

Guest molecule	Concentration with respect to water	Pressure/MPa	
		260 K	270 K
Carbon dioxide	1:6	50	80
	1:8.5	50	80
Methane	1:6	50	80
	1:8.5	50	80

temperature conditions studied are above the three-phase boundary in the phase diagram of carbon dioxide and water. Figs. S3–S8 in ESI cover the snapshots, of cage formation as a function of time and order parameter plots at different pressure and temperature employed in this study. At varying concentration of guest molecules and thermodynamic conditions, we have selected a subset of relevant conditions and presented in the paper. To start with, we selected a pressure of 50 MPa and temperature of 260 K for further investigation within the stability zone for both CH_4 and CO_2 hydrate. Fig. 1 shows the snapshots of the production run of CO_2 and CH_4–water systems (Fig. 1a and b respectively) performed at 260 K and 50 MPa with the different concentrations of guest gases (1:6 and 1:8.5). As can be seen in Fig. 1a, the aqueous phase is well distributed at the beginning of the NPT production run. While at the end of the production run (after 300 ns), the growth of well-arranged hydrate layers on the seed crystal can be observed. Fig. 1b shows the production run of CH_4–water system. As seen in the figure, CH_4 molecules form clusters in the aqueous phase at the start of the production run (0 ns) which is mainly attributed to the hydrophobicity of methane molecules. As shown in the snapshot with both the concentrations (1:6 and 1:8.5), approximately six layers of hydrate have formed on the top of the seed crystal. The partial densities of all the production runs have been presented in the ESI (Fig. S9) which is in good concurrence with the snapshots. Fig. 2 shows the number of cages as a function of time for carbon dioxide and methane

Fig. 2. Evolution of cages (total 5^{12} and $5^{12}6^2$) during simulation. Panel (a) denotes growth of carbon dioxide hydrate and (b) denotes growth of methane hydrate. The data was obtained at a temperature and pressure of 260 K and 50 MPa.

hydrate respectively at 260 K and 50 MPa. It is quite clear that all the four systems show gradual hydrate growth albeit at different rates. On comparing Fig. 2(a) and (b), it is clear that there is a sharp rise in the cage count when we decrease the concentration of carbon dioxide molecules to 1:8.5 which can also be clearly adjudged from the snapshots in Fig. 1(a) and (b). Whereas, the rate of hydrate growth (or the cage count) at different concentrations of methane shows no significant difference as can be seen from Fig. 2(b). The orderness (or extent of hydrate growth) can also be quantified by the use of four body structural order parameter (F_4). It denotes whether the phase is in the hydrate region or in the aqueous phase.

F_4 is defined as $\frac{1}{n}\sum_{i=1}^{n} \cos3\emptyset$ where, n is the number of oxygen–oxygen pairs of water molecules present within 0.3 nm of distance from each other and $\emptyset$ is the torsion angle between them. The average value of F_4 for hydrate system and water is 0.7 and -0.04 respectively [48]. Fig. 3 represents the F_4 order parameter trend with respect to time at 260 K and 50 MPa for both 1:6 and 1:8.5 concentrations of carbon dioxide and methane. The simulation box was divided in equal layers based on the length of a unit cell in order to study the layerwise change in F_4 order parameter. The layer denominations are given in ESI as Fig. S10. A typical increase in the order parameter in Fig. 3(a), has a confirmation of the region proceeding towards the hydrate phase. The region which is just besides the hydrate seed crystal i.e., Layer 1 (red) on both the sides of hydrate seed crystal shows an increase in the order parameter before it progresses to the second layer adjacent to the first layer and so on. This confirms the hypothesis that hydrate growth proceeds in a layerwise fashion [49,50]. From Fig. 3(a), it can be seen that at lower CO_2 concentration, an additional layer of hydrate is formed within the same time frame of 300 ns. Similar trend was also observed for methane hydrate growth (Fig. 3(b)) however the overall hydrate growth of CO_2 hydrate is faster than that of methane hydrate.

As discussed above, all the systems studied above had a tendency for growth towards the hydrate phase at favorable thermodynamic conditions. Interestingly, for some system, no hydrate growth was observed. Fig. 4 (a) shows a snapshot of such a system at 270 K and 50 MPa with a concentration ratio of 1:6 of carbon dioxide molecules at 300 ns. Fig. 4 (b) shows a snapshot of methane hydrate at the same thermodynamic conditions for comparison and it shows sustained hydrate growth with time. At 270 K, even at a pressure as high as 50 MPa, the hydrate phase shows no hydrate growth for CO_2 system. But, if one focuses on methane hydrate at the same thermodynamic conditions in Fig. 4(b), barring a few layers, the hydrate phase growth is complete. This can also be easily inferred if we look at Fig. 5 which denotes the evolution of total number of cages with respect to time. Considering the error bar, the number of cages more or less remains constant with time for the growth of carbon dioxide hydrate while it increases in the case of methane hydrate growth. This unique feature of stunted hydrate growth of CO_2 hydrate at such a high pressure and low temperature can be explained suitably. The factor pertains to the mass transfer limitation in the case of four phase system (liquid water, hydrate water, liquid CO_2 and gaseous CO_2). Under the conditions given (270 K, 50 MPa and 1:6 initial concentration of CO_2), occurrence of CO_2–CO_2 clustering is favorable compared to growth of CO_2 hydrate. Due to the presence of liquid CO_2 and given that the simulation timescale is significantly small, no hydrate growth was observed. To prove the hypothesis, we have conducted experiments wherein the incoming supply of carbon dioxide for hydrate growth is in two phases, one with gaseous CO_2 and another with liquid CO_2. The results of the experiments are plotted in terms of pressure variation in Fig. 6. A pressure drop is seen due to the enclathration of gas molecules in the solid hydrate phase. Rate of the drop in pressure is directly proportional to rate of hydrate growth. As can be observed from Fig. 6, the rate of hydrate formation with liquid CO_2 is gradual compared to that with gaseous CO_2. That is, the hydrate
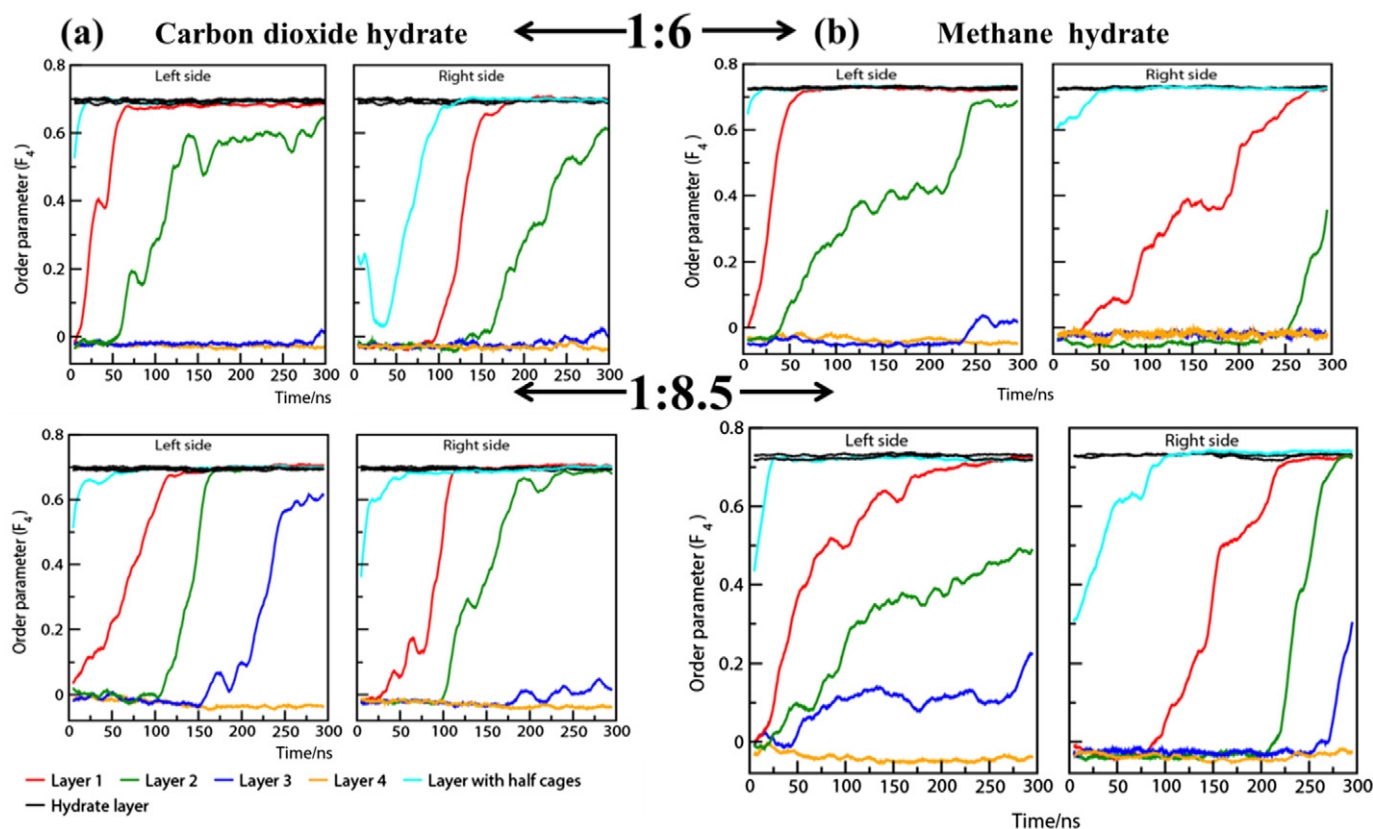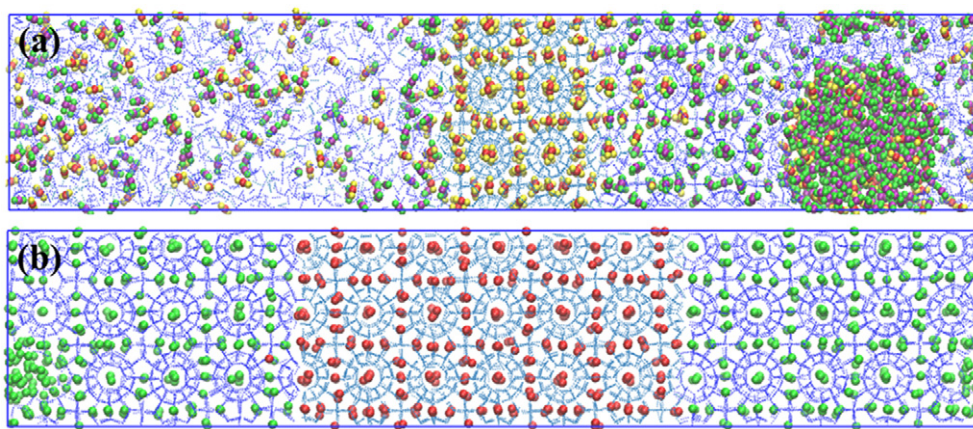

Fig. 3. Order parameter (a) of carbon dioxide hydrate and (b) of methane hydrate plotted in a layerwise fashion at a temperature and pressure of 260 K and 50 MPa. Left and right side denotes the left and right side of the seed crystal in the Z-direction of the simulation box.

Fig. 4. (a) Snapshot of a system at 300 ns with 1:6 concentration of carbon dioxide molecules to water at 270 K and 50 MPa. (Cyan — hydrate water, blue — amorphous water, red and yellow — carbon and oxygen of carbon dioxide in hydrate phase, purple and green — carbon and oxygen of carbon dioxide in amorphous phase.) (b) Snapshot of a system at 300 ns with 1:6 concentration of methane molecules to water at 270 K and 50 MPa. (Red — united atom methane in hydrate phase, green — united atom methane in amorphous phase, cyan — hydrate water, blue — amorphous water.)

formation is slow and is completed in about 10 h from the nucleation point (for liquid CO_2). Whereas the hydrate formation for gaseous CO_2 is completed in about 2.8 h from the onset of nucleation.

Idea behind this work was to identify if the intrinsic kinetics of methane hydrate formation and carbon dioxide formation are of similar time scale or there are certain differences. One may perform experiments in the laboratory setup and compare this, however, the three phase hydrate equilibria of these two systems differ significantly. Thus, it is very difficult to decouple the gas uptake data related to kinetics (arising through the heat and mass transfer limitation) and the thermodynamics (which basically affects the hydrate growth by a factor ($P_{exp} - P_{equ}$)). P_{exp} refers to the experimental pressure at which hydrate growth kinetics is studied, P_{equ} refers to the three phase boundary, and this is the minimum pressure at which a gas–liquid system would convert into a gas–liquid–solid system. The difference $P_{exp} - P_{equ}$ is also known as driving force. Higher pressure in the simulations was chosen for two reasons, at sufficiently high pressure the driving force ($P_{exp} - P_{equ}$) is

going to be almost same for both the system, CO_2/CH_4. Also, the kinetics of hydrate growth would be faster at higher pressure and thus would save computational time. As discussed, in the experiment, the aim was to keep CO_2 in liquid phase and simulate the possibility of CO_2–CO_2 interaction as speculated in the simulation. This was possible around the pressure given (3.6 MPa) and hence we were able to qualitatively compare across the experimental and simulation conditions.

5. Conclusions

In this work, we have studied the intrinsic growth of carbon dioxide and methane hydrate from a seed crystal as a starting point. Growth is studied at different thermodynamic conditions with the combination of two temperatures (260 K & 270 K) and a pressure of 50 MPa. Two suitable concentrations of hydrate-forming gas in the aqueous phase (1:6, 1:8.5) are then chosen for NPT ensemble as a production run for molecular dynamics simulation. A total of sixteen systems were investigated for the growth of carbon dioxide and methane hydrate. Based on the four body structural order parameter (F_4) and the number of cages which originated during the growth process we witnessed sustained growth of the seed crystal for all the methane hydrate system (irrespective of methane concentration in the aqueous phase).

However, with the system involving the growth of carbon dioxide hydrate, hydrate growth rate decreased with respect to the increase of concentration of the guest molecules in the aqueous phase. Moreover, at 50 MPa and 270 K the system with a higher concentration ratio of 1:6 (gas to water) witnessed no hydrate growth. It was observed that at these thermodynamic conditions, CO_2 clustering was favored over hydrate growth. At lower CO_2 to water concentration (1:8.5), the trend of hydrate growth was on expected line and hydrate continued to grow with time as expected. An investigation was done to reveal the reason behind this behavior. We carried out experiments pertaining to incoming flow of gaseous and liquid CO_2 and observe its effects on the growth of CO_2 hydrate. We saw that the rate of hydrate growth is clearly dependent on the state of CO_2 that is supplied. The above result clearly shows that replacing methane from natural gas hydrate reservoir requires an optimum initial concentration of CO_2 in the aqueous phase so that the phase separation is not predominant for the desired result.
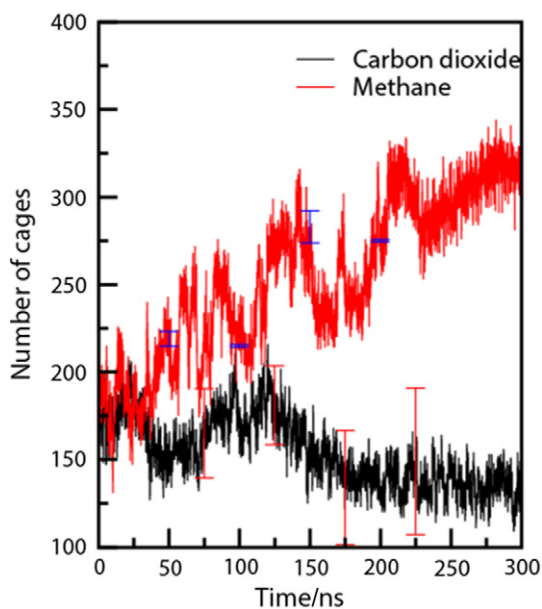
Fig. 5. Evolution of cages (total 5^{12} and $5^{12}6^2$) during simulation. The black and red curve is at a temperature and pressure of 270 K 50 MPa and a concentration of 1:6 with respect to water.
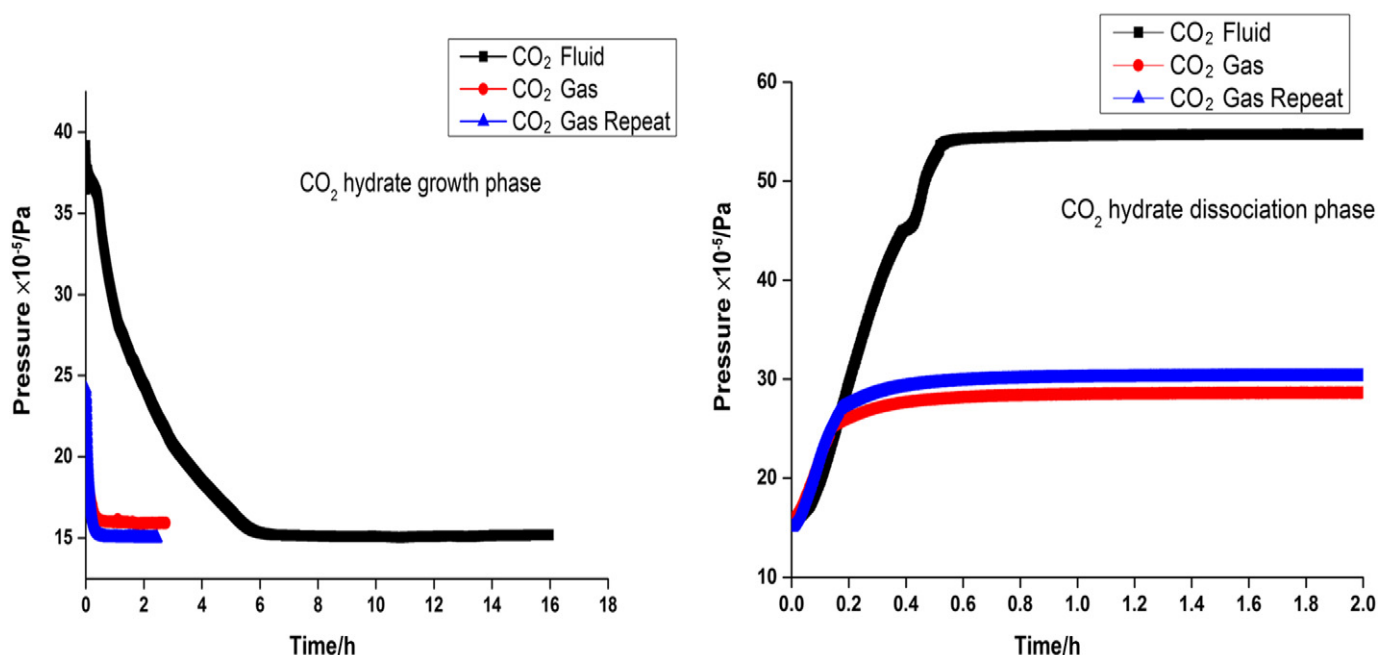
Fig. 6. Hydrate growth (a) and dissociation curves (b) for CO_2 hydrate under conditions resembling gaseous and liquid CO_2.

Supplementary Material

Supplementary data to this article can be found online at https://doi.org/10.1016/j.cjche.2019.02.006.

References

[1] C.A. Koh, Towards a fundamental understanding of natural gas hydrates, *Chem. Soc. Rev.* 31 (2002) 157–167.
[2] E.D. Sloan, C. Koh, Clathrate Hydrates of Natural Gases, Third edition CRC Press, 2007.
[3] C.A. Koh, R.P. Wisbey, X. Wu, R.E. Westacott, A.K. Soper, Water ordering around methane during hydrate formation, *J. Chem. Phys.* 113 (2000) 6390–6397.
[4] D.-Y. Koh, H. Kang, J. Jeon, Y.-H. Ahn, Y. Park, H. Kim, H. Lee, Tuning cage dimension in clathrate hydrates for hydrogen multiple occupancy, *J. Phys. Chem. C* 118 (2014) 3324–3330.
[5] A. Lenz, L. Ojamae, Structures of the I-, II- and H-methane clathrates and the ice–methane clathrate phase transition from quantum-chemical modeling with force-field thermal corrections, *J. Phys. Chem. A* 115 (2011) 6169–6176.
[6] R. Susilo, S. Alavi, J.A. Ripmeester, P. Englezos, Molecular dynamics study of structure H clathrate hydrates of methane and large guest molecules, *J. Chem. Phys.* 128 (2008) 194505.
[7] H. Komatsu, M. Ota, R.L. Smith Jr., H. Inomata, Review of CO_2–CH_4 clathrate hydrate replacement reaction laboratory studies — Properties and kinetics, *J. Taiwan Inst. Chem. Eng.* 44 (2013) 517–537.
[8] J. Zhao, K. Xu, Y. Song, W. Liu, W. Lam, Y. Liu, K. Xue, Y. Zhu, X. Yu, Q. Li, A review on research on replacement of CH_4 in natural gas hydrates by use of CO_2, *Energies* 5 (2012) 399–419.
[9] N. Goel, In situ methane hydrate dissociation with carbon dioxide sequestration: Current knowledge and issues, *J. Pet. Sci. Eng.* 51 (2006) 169–184.
[10] S. Lombardi, L.K. Altunina, S.E. Beaubien, Advances in the Geological Storage of Carbon Dioxide: International Approaches to Reduce Anthropogenic Greenhouse Gas Emissions, Springer, Netherlands, 2006.
[11] L.P. Hauge, K.A. Birkedal, G. Ersland, A. Graue, Methane Production from Natural Gas Hydrates by CO_2 Replacement — Review of Lab Experiments and Field Trial, SPE Bergen One Day Seminar, Society of Petroleum Engineers, 2014, https://doi.org/10.2118/169198-MS.
[12] H. Lee, Y. Seo, Y.-T. Seo, I.L. Moudrakovski, J.A. Ripmeester, Recovering methane from solid methane hydrate with carbon dioxide, *Angew. Chem.* 115 (2003) 5202–5205.
[13] S. Lee, S. Park, Y. Lee, Y. Seo, Thermodynamic and 13C NMR spectroscopic verification of methane–carbon dioxide replacement in natural gas hydrates, *Chem. Eng. J.* 225 (2013) 636–640.
[14] D.Q. Robert, W. Hawtin, P. Mark Rodger, Gas hydrate nucleation and cage formation at a water/methane interface, *Phys. Chem. Chem. Phys.* 10 (2008) 4853–4864.
[15] M.R. Walsh, G.T. Beckham, C.A. Koh, E.D. Sloan, D.T. Wu, A.K. Sum, Methane hydrate nucleation rates from molecular dynamics simulations: Effects of aqueous methane concentration, interfacial curvature, and system size, *J. Phys. Chem. C* 115 (2011) 21241–21248.
[16] M.R. Walsh, J.D. Rainey, P.G. Lafond, D.-H. Park, G.T. Beckham, M.D. Jones, K.-H. Lee, C.A. Koh, E.D. Sloan, D.T. Wu, A.K. Sum, The cages, dynamics, and structuring of incipient methane clathrate hydrates, *Phys. Chem. Chem. Phys.* 13 (2011) 19951.
[17] C.T. Moon, P.C. Taylor, P.M. Rodger, Molecular dynamics study of gas hydrate formation, *J. Am. Chem. Soc.* 125 (2003) 4706–4707.
[18] J.K. Vatamanu, P.G. Kusalik, Molecular insights into the heterogeneous crystal growth of sI methane hydrate, *J. Phys. Chem. B* 110 (2006) 15896–15904.
[19] J.P.L. Lederhos, J.P., A. Sum, R.L. Christiansen, E.D. Sloan, Effective kinetic inhibitors for natural gas hydrates, *Chem. Eng. Sci.* 51 (1995) 1221–1229.
[20] J.D. Lee, P. Englezos, Unusual kinetic inhibitor effects on gas hydrate formation, *Chem. Eng. Sci.* 61 (2006) 1368–1376.
[21] A. Kumar, G. Bhattacharjee, B.D. Kulkarni, R. Kumar, Role of surfactants in promoting gas hydrate formation, *Ind. Eng. Chem. Res.* 54 (49) (2015) 12217–12232.
[22] M.R. Walsh, C.A. Koh, E.D. Sloan, A.K. Sum, D.T. Wu, Microsecond simulations of spontaneous methane hydrate nucleation and growth, *Science* 326 (2009) 1095–1098.
[23] S. Sarupria, P.G. Debenedetti, Homogeneous nucleation of methane hydrate in microsecond molecular dynamics simulations, *J. Phys. Chem. Lett.* 3 (2012) 2942–2947.
[24] H. Nada, Growth mechanism of a gas clathrate hydrate from a dilute aqueous gas solution: A molecular dynamics simulation of a three-phase system, *J. Phys. Chem. B* 110 (2006) 16526–16534.
[25] Y.-T. Tung, L.-J. Chen, Y.-P. Chen, S.-T. Lin, The growth of structure I methane hydrate from molecular dynamics simulations, *J. Phys. Chem. B* 114 (2010) 10804–10813.
[26] G. Tegze, T. Pusztai, G. Toth, L. Granasy, A. Svandal, T. Buanes, T. Kuznetsova, B. Kvamme, Multiscale approach to CO_2 hydrate formation in aqueous solution: Phase field theory and molecular dynamics. Nucleation and growth, *J. Chem. Phys.* 124 (2006) 234710.
[27] Y.-T. Tung, L.-J. Chen, Y.-P. Chen, S.-T. Lin, Growth of structure I carbon dioxide hydrate from molecular dynamics simulations, *J. Phys. Chem. C* 115 (2011) 7504–7515.
[28] Z. He, P. Linga, J. Jiang, What are the key factors governing the nucleation of CO_2 hydrate? *Phys. Chem. Chem. Phys.* 19 (2017) 15657–15661.
[29] S. Sarupria, P.G. Debenedetti, Molecular dynamics study of carbon dioxide hydrate dissociation, *J. Phys. Chem. A* 115 (2011) 6102–6111.
[30] P. Linga, N. Daraboina, J.A. Ripmeester, P. Englezos, Enhanced rate of gas hydrate formation in a fixed bed column filled with sand compared to a stirred vessel, *Chem. Eng. Sci.* 68 (2012) 617–623.
[31] I.L. Moudrakovski, G.E. McLaurin, C.I. Ratcliffe, J.A. Ripmeester, Methane and carbon dioxide hydrate formation in water droplets: Spatially resolved measurements from magnetic resonance microimaging, *J. Phys. Chem. B* 108 (2004) 17591–17595.
[32] B.K. Hess, C., D. Van der Spoel, E. Lindahl, GROMACS: Algorithms for highly efficient, load-balanced and scalable molecular simulation, *J. Chem. Theory Comput.* 4 (2008) 435–447.

[33] M.M. Conde, C. Vega, Determining the three-phase coexistence line in methane hydrates using computer simulations, *J. Chem. Phys.* 133 (2010), 064507.

[34] M.M. Conde, C. Vega, Note: A simple correlation to locate the three phase coexistence line in methane-hydrate simulations, *J. Chem. Phys.* 138 (2013), 056101.

[35] J.G.Y. Harris, K.H. Yung, Carbon dioxide's liquid–vapor coexistence curve and critical properties as predicted by a simple molecular model, *J. Phys. Chem.* 99 (1995) 12021–12024.

[36] K. Watanabe, H. Okajima, T. Kato, H.O. Hamaguchi, Rotational dynamics of solvated carbon dioxide studied by infrared, Raman, and time-resolved infrared spectroscopies and a molecular dynamics simulation, *J. Chem. Phys.* 136 (2012), 014508.

[37] J.I.S. Marcus, G. Martin, Transferable potentials for phase equilibria. 1. United-atom description of n-alkanes, *J. Phys. Chem.* 102 (1998) 2569–2577.

[38] B. Hess, H. Bekker, H.J.C. Berendsen, J.G.E.M. Fraaije, LINCS: A linear constraint solver for molecular simulations, *J. Comput. Chem.* 18 (1997) 1463–1472.

[39] T.Y. Darden, D., L. Pedersen, Particle mesh Ewald: An N.log(N) method for Ewald sums in large systems, *J. Chem. Phys.* 98 (1993) 10089.

[40] U.P. Essmann, L., M.L. Berkowitz, T. Darden, H. Lee, L.G. Pedersen, A smooth particle mesh Ewald method, *J. Chem. Phys.* 103 (1995) 8577.

[41] W.G. Hoover, Canonical dynamics: Equilibrium phase-space distributions, *Phys. Rev. A* 31 (1985) 1695–1697.

[42] S. Nose, A unified formulation of the constant temperature molecular dynamics methods, *J. Chem. Phys.* 81 (1984) 511–519.

[43] S. Nose, M.L. Klein, Constant pressure molecular dynamics for molecular systems, *Mol. Phys.* 50 (1983) 1055–1076.

[44] M.R. Parrinello, A. Rahman, Polymorphic transitions in single crystals: A new molecular dynamics method, *J. Appl. Phys.* 52 (1981) 7182–7190.

[45] L.C. Jacobson, W. Hujo, V. Molinero, Thermodynamic stability and growth of guest-free clathrate hydrates: A low-density crystal phase of water, *J. Phys. Chem. B* 113 (2009) 10298–10307.

[46] M. Matsumoto, A. Baba, I. Ohmine, Topological building blocks of hydrogen bond network in water, *J. Chem. Phys.* 127 (2007) 134504.

[47] F. Jiménez-Ángeles, A. Firoozabadi, Nucleation of methane hydrates at moderate subcooling by molecular dynamics simulations, *J. Phys. Chem. C* 118 (2014) 11310–11318.

[48] C. Moon, R.W. Hawtin, P.M. Rodger, Nucleation and control of clathrate hydrates: Insights from simulation, *Faraday Discuss.* 136 (2007) 367.

[49] V.S. Baghel, R. Kumar, S. Roy, Heat transfer calculations for decomposition of structure I methane hydrates by molecular dynamics simulation, *J. Phys. Chem. C* 117 (2013) 12172–12182.

[50] S. Das, V.S. Baghel, S. Roy, R. Kumar, A molecular dynamics study of model SI clathrate hydrates: The effect of guest size and guest–water interaction on decomposition kinetics, *Phys. Chem. Chem. Phys.* 17 (2015) 9509–9518.